Differential responses of hippocampal subfields to cortical up–down states

Thomas T. G. Hahn*, Bert Sakmann*, and Mayank R. Mehta†‡

*Department of Cell Physiology, Max Planck Institute for Medical Research, D-69120 Heidelberg, Germany; and †Department of Neuroscience, Brown University, Providence, RI 02912

Communicated by Mortimer Mishkin, National Institutes of Health, Bethesda, MD, January 9, 2007 (received for review October 9, 2006)

The connectivity of the hippocampal trisynaptic circuit, formed by the dentate gyrus, the CA3 and the CA1 region, is well characterized anatomically and functionally *in vitro*. The functional connectivity of this circuit *in vivo* remains to be understood. Toward this goal, we investigated the influence of the spontaneous, synchronized oscillations in the neocortical local field potential, reflecting up–down states (UDS) of cortical neurons, on the hippocampus. We simultaneously measured the extracellular local field potential in association cortex and the membrane potential of identified hippocampal excitatory neurons in anesthetized mice. Dentate gyrus granule cells showed clear UDS modulation that was phase locked to cortical UDS with a short delay. In contrast, CA3 pyramidal neurons showed mixed UDS modulation, such that some cells were depolarized during the cortical up state and others were hyperpolarized. CA1 pyramidal neurons, located farther downstream, showed consistent UDS modulation, such that when the cortical and dentate gyrus neurons were depolarized, the CA1 pyramidal cells were hyperpolarized. These results demonstrate the differential functional connectivity between neocortex and hippocampal subfields during UDS oscillations.

consolidation | hippocampus | neocortex | oscillation | sleep

Cortico-hippocampal interaction, especially during quiet wakefulness and sleep, is thought to be important for the formation of long-term memories by a process of consolidation (1–12). During these behavioral states and under anesthesia, neocortical neurons are spontaneously active, and their activity is modulated by slow, 0.3- to 1.5-Hz oscillations called up–down states (UDS) characteristic of slow wave sleep (SWS) oscillations. Both the local field potential (LFP) and the membrane potential (MP) show that UDS are synchronized across large areas of the cortex (13–17). Although neocortex is the major source of input to the hippocampal formation (18), the hippocampal LFP shows large-irregular activity during SWS that seems uncorrelated with the neocortical activity (19, 20). This is indicative of minimal cortico-hippocampal interaction during UDS. However, recent studies have shown cortico-hippocampal interaction during various behavioral states including SWS (6, 11, 21–26). The mechanisms underlying this interaction and the contribution of different parts of the hippocampal circuit to this interaction remain to be understood.

Each area of the hippocampal trisynaptic circuit sends glutamatergic projections to both excitatory and inhibitory neurons in the next stage (27). Hence, the net output of any hippocampal region would be a complex and, presumably, state-dependent function of the strength and timing of excitatory and inhibitory inputs (28). The functional connectivity of cortico-hippocampal circuits has been extensively investigated by using electrical stimulation [see e.g., special issue of *Hippocampus* (1995) 5:101–146], whereas its interrelations with spontaneous activity such as UDS have received little attention so far.

We hypothesized that the large and synchronous UDS activity in neocortex during SWS should have a substantial impact on the activity of hippocampal neurons. Further, given the long duration of UDS (0.5–2 s) with rapid transitions between the states, we hypothesized that the UDS transitions could be used to quantify the functional connectivity of the cortico-hippocampal circuit by measuring the membrane potential of hippocampal neurons in relation to the UDS.

Toward this goal, we made *in vivo* whole-cell measurements of the MP of principal neurons from the three hippocampal subdivisions in 33 urethane-anesthetized mice. Simultaneously, using LFP recordings, we monitored the UDS activity of layer 2/3 of the parietal association cortex, representative of neocortical inputs to the hippocampal formation, which in turn projects to all regions of the hippocampus (18, 27). Specifically we measured the MP of 10 dentate gyrus granule cells, 10 dorsal CA3 pyramidal neurons, and 13 dorsal CA1 pyramidal neurons. We found that these principal neurons in the three subfields of the hippocampus responded differentially during UDS, indicative of differential functional coupling during UDS.

Results

Average Membrane Potential Is Significantly Different Among Dentate Gyrus, CA1, and CA3. The average MP of dentate gyrus granule cells was -62.7 ± 2.5 mV (mean ± SEM). They were significantly less depolarized than CA1 pyramidal neurons (-51.2 ± 2.3 mV, $P = 0.003$) and CA3 pyramidal neurons (-48.2 ± 2.6 mV, $P = 0.001$) (see *Methods*). The spontaneous firing rates of principal neurons in these three regions followed a pattern consistent with the level of their MP values. Granule cells had the lowest median spike rate (0.005 ± 0.03 Hz). Most granule cells fired only a couple of spikes or none during the experiment. Firing rates were higher in CA1 (0.14 ± 0.11 Hz, $P = 0.03$) and CA3 pyramidal neurons (0.17 ± 0.12 Hz, $P = 0.08$). The pattern of spiking across the three hippocampal subfields is consistent with extracellular measurements in anesthetized (29) and normally sleeping rodents (30, 31). The extracellular firing rates are higher than the above values, probably because extracellular measurements may not detect the activity of silent or very low spike-rate cells.

Dentate Gyrus Granule Cells Are Phase Locked to Cortical UDS. Granule cells receive their primary afferents from the entorhinal cortex (18, 27). They showed clear UDS modulation with prolonged down states and sharp transitions to episodes of depolarization (Fig. 1 *a* and *b*). Whereas the down states were clearly seen in granule cells, episodes of depolarization were of smaller amplitude and shorter duration compared with up states

This work was presented in part at the 2006 Society of Neuroscience Meeting, Atlanta, GA, October 14, 2006.

Author contributions: T.T.G.H. and M.R.M. designed research; T.T.G.H. and M.R.M. performed research; M.R.M. analyzed data; and T.T.G.H., B.S., and M.R.M. wrote the paper.

The authors declare no conflict of interest.

Abbreviations: AP, action potential; LFP, local field potential; MP, membrane potential; SWS, slow wave sleep; UDS, up–down states.

‡To whom correspondence should be addressed. E-mail: mayank@brown.edu.

This article contains supporting information online at www.pnas.org/cgi/content/full/0700222104/DC1.

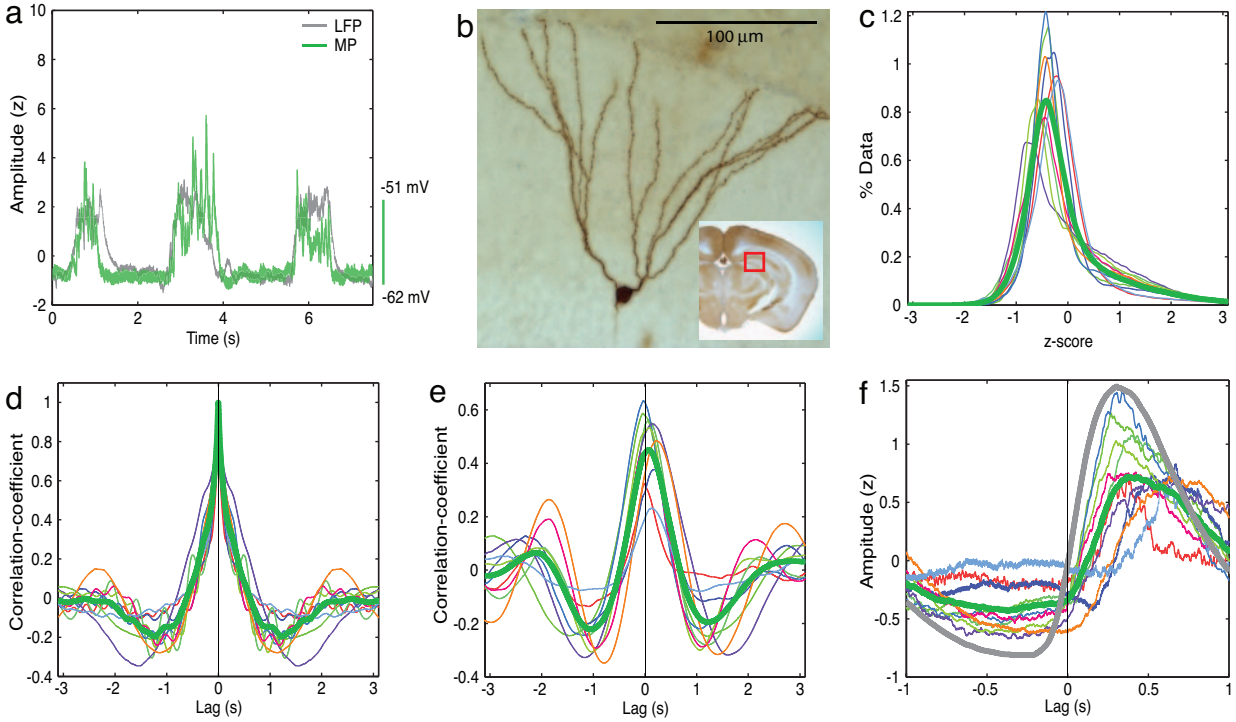

Fig. 1. Phase locking of dentate gyrus granule cells' MP to cortical UDS. (*a*) UDS in the simultaneously recorded neocortical layer two/three LFP (gray) and a granule cells' MP (green). To allow numerical comparison of the depth of the UDS across different conditions, the units of LFP and MP were converted from volts to *z* score in all of the figures, and the LFP was multiplied by −1 (see *Methods*). (*b*) Micrograph of the granule cell from which the MP in *a* was recorded. (*Inset*) The approximate anatomical location of the neuron in a representative coronal section. (*c*) MP histogram. In this and all subsequent histograms, thin lines of different colors represent data from single experiments (same colors refer to the same experiments within a figure). The thick green line denotes the ensemble-averaged MP histogram. The histograms show a large peak at negative values, indicating the down state, and a small tail at positive values, indicating the presence of UDS. (*d*) MP autocorrelations show a slow oscillation of ≈0.5 Hz UDS, with a significant trough of ≈1.24 s (-0.2 ± 0.03; $P = 3e^{-5}$, *t* test; $P = 9e^{-4}$, binomial test). (*e*) MP–LFP correlation. The MP–LFP covariance is shown as a function of time lag. Covariance was high at zero latency 0.44 ± 0.08 ($P = 4e^{-6}$), with the maximum value of population averaged covariance occurring at 76 ms, indicating that the granule cell's MP followed cortical LFP. (*f*) LFP-triggered MP. All recorded neurons show rapid depolarization upon transition to up-state in the LFP. For comparison, the averaged LFP-triggered LFP is shown by a gray trace. The average peak of LFP-triggered MP reaches a maximum value of 0.72 at 67 ms after cortical LFP reaches a maximum, which indicates a strong phase-locking of dentate granule cells' MP to cortical UDS with a small delay.

in neocortical LFP, as evidenced by the MP histogram, which showed a larger fraction of data points to the left of the origin corresponding to the down state, and very little data to the right corresponding to depolarizations (Fig. 1*c*). The rhythmic component of UDS modulation of granule cells' activity was quantified by computing the autocorrelation of the MP (Fig. 1*d*). The population averaged autocorrelation showed a strong and highly significant trough at 1.24 s (-0.2 ± 0.03, $P = 3e^{-5}$, *t* test; $P = 9e^{-4}$, binomial test), indicative of strong ≈0.5-Hz UDS modulation.

This modulation could be either related to the neocortical UDS or be unrelated to it. To quantify the relationship between the granule cells' activity and the neocortical UDS, we computed the cross-correlation between the granule cells' MP and neocortical LFP (Fig. 1*e*). The MP–LFP correlation was highly significant and positive at zero latency for all granule cells (0.44 ± 0.08, $P = 4e^{-6}$, *t* test; $P = 9e^{-4}$, binomial test). Furthermore, the maximum of the average MP–LFP correlation occurred at 76 ± 28 ms, which was significantly greater than 0 ms ($P = 0.01$). Because cortical neurons show ≈0.5-Hz UDS, with the spiking activity reaching a maximum of approximately zero phase lag with respect to the LFP (32), our data indicate that the granule cells' MP followed neocortical UDS with a small phase lag.

Although the cross-correlation provides accurate information about the overall relationship between MP and LFP, it does not capture the change in MP around the time when the LFP makes transitions between up and down states. This problem arises because these transitions are very rapid, with the LFP being mostly constant in either the up or the down state. To estimate the precise timing of granule cells' activity with respect to neocortical UDS transitions, we computed the average value of the granule cells' MP around the time when the neocortical LFP made a transition from the down to the up state (LFP-triggered MP). For comparison, we also computed the average value of the LFP around the same transition points (LFP-triggered LFP). The average LFP-triggered MP showed a clear and rapid increase in depolarization for all granule cells (Fig. 1*f*). Furthermore, in all cases, the LFP-triggered MP underwent a rapid depolarizing transition after the cortical LFP made that transition ($P = 9e^{-4}$, binomial test). The population-averaged, LFP-triggered MP reached a maximal value of 0.72 ± 0.13, which was significantly greater than zero ($P = 3e^{-7}$) but significantly smaller than LFP-triggered LFP's maximal value (1.5 ± 0.03, $P = 2.5e^{-11}$), suggesting that the UDS modulation of granule cells was weaker than that of the neocortical LFP. Furthermore, the maximum of the ensemble averaged LFP-triggered MP occurred at 374 ms, whereas that for the LFP-triggered LFP occurred at 307 ms. Thus, the granule cells were rapidly depolarized 67 ms after the cortical LFP made a transition to the up state. This finding is consistent with the above result of the MP–LFP correlation timing and further supports the hypothesis that granule cells' UDS-related activity is driven by cortical inputs.

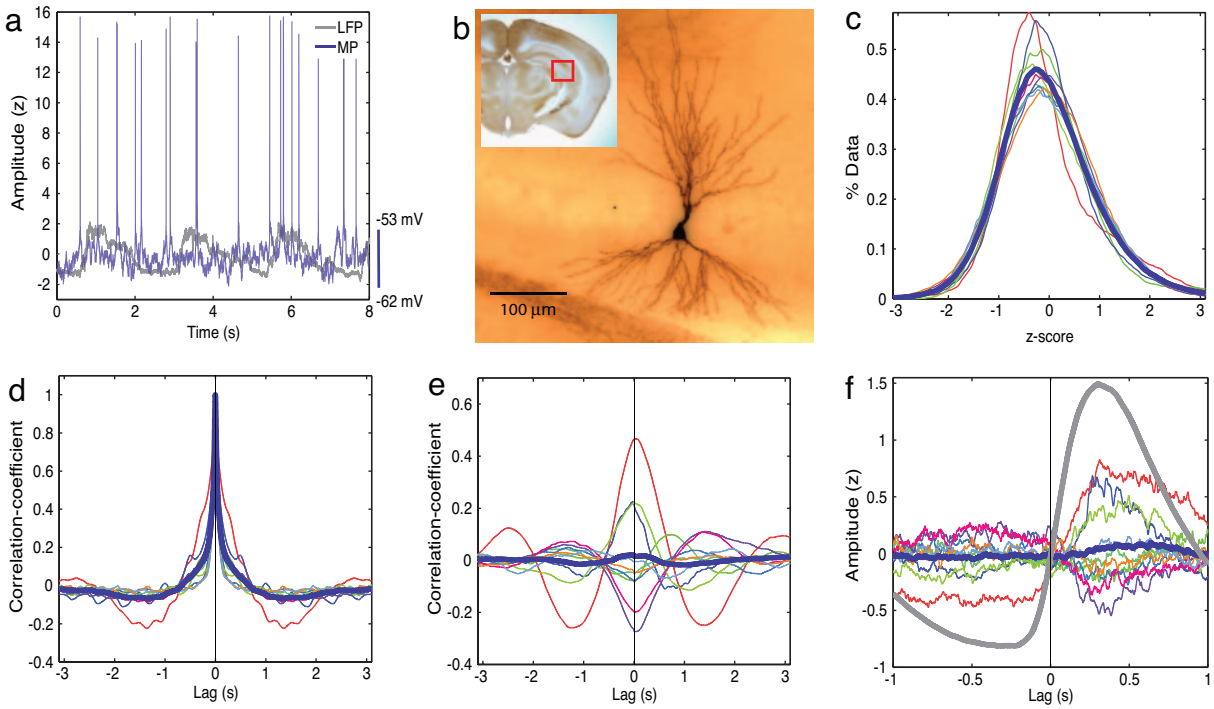

Fig. 2. Weak and mixed UDS responses of CA3 pyramidal neurons. (*a*) UDS in simultaneously recorded neocortical LFP (gray) and CA3 pyramidal neuron's MP (blue). The units are as in Fig. 1. (*b*) Micrograph of the CA3 pyramidal neuron from which MP in *a* was recorded. (*c*) MP histograms showing unimodal distribution for individual experiments (colored lines) and population average (thick blue line), indicative of an absence of UDS. (*d*) Autocorrelations of MPs show small but significant UDS modulation with a very small but significant trough of ≈1.36 s (-0.07 ± 0.02, $P = 7e^{-3}$). (e) The MP–LFP correlation varies substantially across different neurons (colored lines), such that the population average (thick blue line) showed insignificant correlation. (*f*) The LFP-triggered MP showed variable UDS modulation (colored lines), with the population average (thick blue line) showing no significant UDS modulation.

CA3 Pyramidal Neurons Show Significant but Mixed UDS Modulation. The granule cells project onto both excitatory and inhibitory neurons in CA3. CA3 neurons also receive inputs directly from the entorhinal cortex and have strong recurrent connections. Although granule cells showed strong UDS modulation synchronous with cortical UDS, CA3 pyramidal neurons showed much weaker UDS modulation (Fig. 2 *a* and *b*). This finding was evidenced by a unimodal distribution of the MP (Fig. 2*c*) and a significant but very weak trough in the autocorrelation of MP at 1.36 s (-0.07 ± 0.02, $P = 7e^{-3}$) (Fig. 2*d*).

Although the MP did not show strong UDS modulation, its fluctuations may be correlated with neocortical UDS. Indeed, the MP–LFP correlations showed disparate behavior across different CA3 neurons, exhibiting both positive and negative correlations (Fig. 2*e*). The population averaged MP–LFP correlation did not show significant correlation with cortical UDS (0.02 ± 0.07, $P = 0.8$). The LFP-triggered MP also showed similar results (Fig. 2*f*) and an insignificant change in the population-averaged MP after a neocortical transition to the up state. However, the MP of individual CA3 neurons showed significant UDS modulation. Modulation was quantified by splitting up the data for each cell in 20 segments and computing the significance of the distribution of correlations in these 20 segments at zero latency. Thus, even though the average CA3 behavior exhibited no clear UDS modulation, 9 of 10 CA3 neurons showed significant ($P < 0.01$) modulation, of which 3 CA3 neurons were significantly more depolarized in the up state and 6 were significantly less depolarized. It is conceivable that these neurons formed functionally different subgroups.

CA1 Pyramidal Neurons Are Less Depolarized During Cortical Up States. Pyramidal neurons in CA1 receive glutamatergic inputs from the entorhinal cortex (27) and from CA3. CA1 pyramidal neurons typically showed weak UDS modulation (Fig. 3 *a* and *b*) such that the MP tended to be less depolarized when the neocortex was more depolarized (up state). However, the neurons did not show clear UDS, as evidenced by unimodal distribution of the MP (Fig. 3*c*) and by a significant but weak UDS trough in the MP autocorrelation at 1.25 s (-0.1 ± 0.01, $P = 2e^{-6}$) (Fig. 3*d*). Notably, despite a lack of UDS in the MP, the MP–LFP cross-correlation showed a significant UDS modulation (Fig. 3*e*). The MP–LFP correlation was significantly negative for all CA1 pyramidal neurons (-0.21 ± 0.08; $P = e^{-7}$, *t* test; $P = 1e^{-4}$, binomial test). Thus the CA1 pyramidal cells' MP was anticorrelated with cortical UDS, i.e., they became less depolarized during cortical up states. Furthermore, unlike the autocorrelation, the MP–LFP correlation showed clear UDS rhythmicity (Fig. 3*e*). The strongest anticorrelation between cortical LFP and CA1 pyramidal cells' MP occurred at 26 ± 5 ms. The anticorrelation was further corroborated by the LFP-triggered MP, which displayed hyperpolarization with a minimum value of -0.31 ± 0.05 ($P = 4e^{-5}$) after the down-to-up transition in the LFP. These results demonstrate that CA1 pyramidal neurons show weak but consistent UDS modulation, such that they are less depolarized during cortical up states.

Discussion

The response properties of hippocampal principal neurons in dentate gyrus, CA3, and CA1 were substantially different during cortical UDS. Whereas cortical LFP displayed strong UDS modulation, resulting in a bimodal distribution of LFP (Fig. 4*a*), granule cells' MP showed a weak bimodality, and the MP of CA3 and CA1 pyramidal cells was unimodally distributed (Fig. 4*a*). The autocorrelation of neocortical LFP showed the strongest and most significant UDS modulation (Fig. 4*b*). The granule cells' MP autocorrelations showed weaker but significant UDS

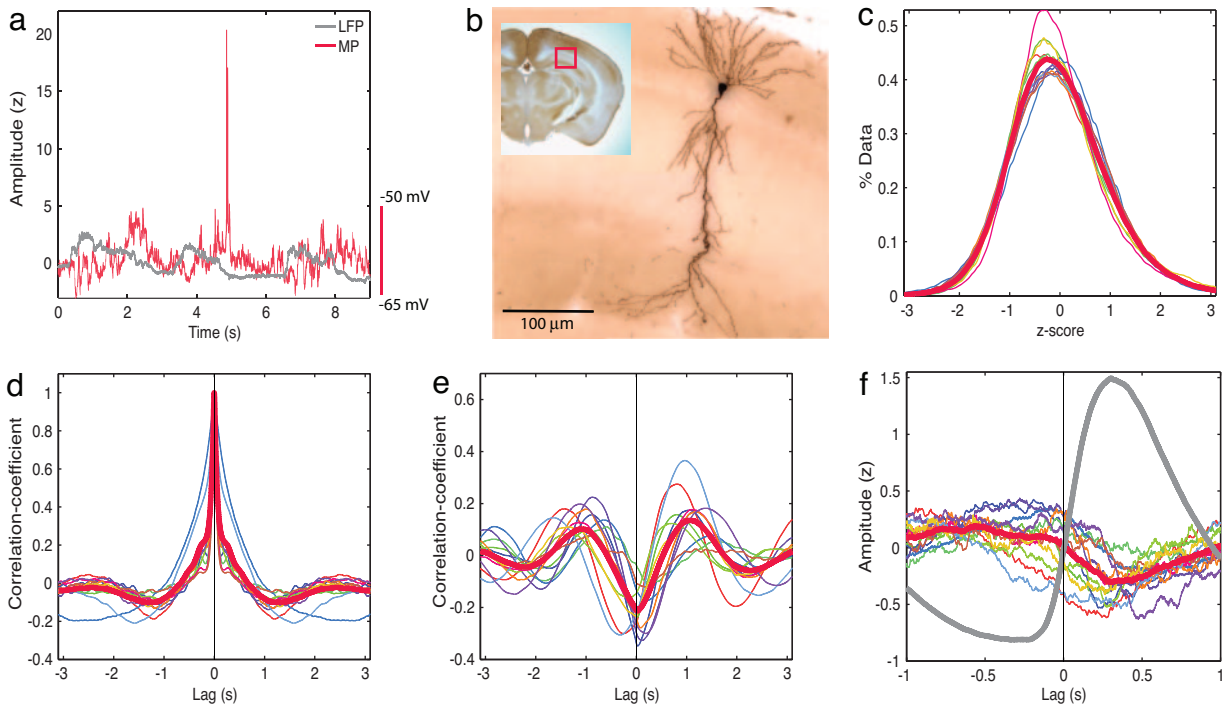

Fig. 3. Reduced depolarization of CA1 pyramidal neurons during cortical up state. (*a*) Neocortical LFP (gray) shows UDS, but the CA1 pyramidal neuron's MP (red) does not. The units are as in Fig. 1. (*b*) The CA1 pyramidal neuron from which MP shown in *a* was recorded. (*c*) MP histograms of individual cells (colored lines) and population average (thick red line) are unimodal, indicating the absence of UDS. (*d*) MP autocorrelations indicate a small but highly significant trough at 1.25 s (-0.1 ± 0.01, $P = 2e^{-6}$), indicating clear UDS modulation. (*e*) The MP–LFP cross-correlation between CA1 pyramidal cells' MP and the cortical LFP was significantly negative at zero latency (-0.21 ± 0.08, $P = e^{-7}$), indicating significant anticorrelation between MP and LFP. (*f*) The LFP-triggered MP shows clear UDS modulation with the population average (thick red line) attaining a minimum value of -0.31 ± 0.05 ($P = 4e^{-5}$) at 312 ms. Thus, CA1 pyramidal neurons show weak phase locking with cortical UDS, such that when cortex is in the up state, CA1 pyramidal neurons are less depolarized.

modulation, whereas CA3 and CA1 pyramidal neurons' autocorrelations also displayed significant but much weaker UDS modulation.

The dorsal CA1 LFP was bimodally distributed [supporting information (SI) Fig. 5] and strongly correlated with parietal cortical LFP (0.8 ± 0.02, $P = 7e^{-41}$). Granule cells were phase locked to cortical LFP with a phase lag of 76 ms. CA3 pyramidal neurons' MP showed significant but mixed correlations with cortical UDS. CA1 pyramidal neurons were consistently negatively correlated with cortical LFP, with the lowest correlation occurring at 26 ms. Qualitatively similar results were obtained when action potentials from the recorded neurons were analyzed (SI Fig. 6) instead of the subthreshold membrane potential data in the above computations.

Analogous differential responses were seen with LFP-triggered MP. Cortical LFP showed a rapid transition from down to up state. Granule cells showed a rapid depolarization 67 ms after the cortical LFP made a transition to the up state. Some CA3 pyramidal cells were more depolarized after the onset of cortical up state, whereas most of them were significantly less depolarized during cortical up state. All CA1 pyramidal cells were significantly less depolarized during the cortical up state.

Anatomical and electrophysiological work identifies entorhinal cortex as the major source of synaptic input to all parts of hippocampus. The rapid depolarization of granule cells' MP briefly after a transition to the up state in neocortex suggests that the MP of granule cells is primarily governed by cortical inputs. Pyramidal neurons in CA3 receive glutamatergic inputs from the entorhinal cortex and from the granule cells. CA3 pyramidal neurons have extensive recurrent connections. Inputs to CA3 also terminate on GABAergic interneurons, which in turn project to CA3 pyramidal neurons. Because the granule cells had very low spiking rates in our experiments, the activity of CA3 during UDS is likely determined by direct entorhinal inputs and by recurrent connections within CA3. The CA3 pyramidal neurons receiving stronger entorhinal inputs or stronger recurrent inputs compared with recurrent inhibitory inputs would show increased depolarization after the up state transition in the cortex. Those CA3 pyramidal neurons receiving stronger inputs from CA3 interneurons than from the entorhinal or the recurrent inputs would show reduced depolarization after a transition to up state in the cortex (33).

Similar mechanisms could explain reduced depolarization in CA1 pyramidal cells during cortical up state (34). Very low levels of recurrent excitatory connections within CA1 could generate a more homogenous behavior of the CA1 pyramids than in CA3 and reduced depolarization during the up state. This mechanism would require that interneurons in CA3 and CA1 respond in a phase-locked fashion to cortical UDS. We recently showed that R-LM interneurons in CA1 indeed show clear UDS that are phase locked to cortical LFP with a short delay (35). Similar results may hold for CA3 interneurons. Reduced feed-forward inhibition during the down state might further influence CA1 and CA3 activity by releasing recurrent excitation within CA3, which in turn can contribute to CA3 and upstream CA1 depolarization.

Several other mechanisms might be involved in the differential activity of hippocampal subfields during UDS. For example, medial septal neurons provide strong GABAergic projections to all parts of the hippocampus. The relationship of medial septal neurons' activity to UDS is unknown. Furthermore, although neocortical neurons are synchronized during UDS (13–17), neurons in entorhinal projection neurons to the three hippocampal subregions may spike at different phases of UDS. Further-

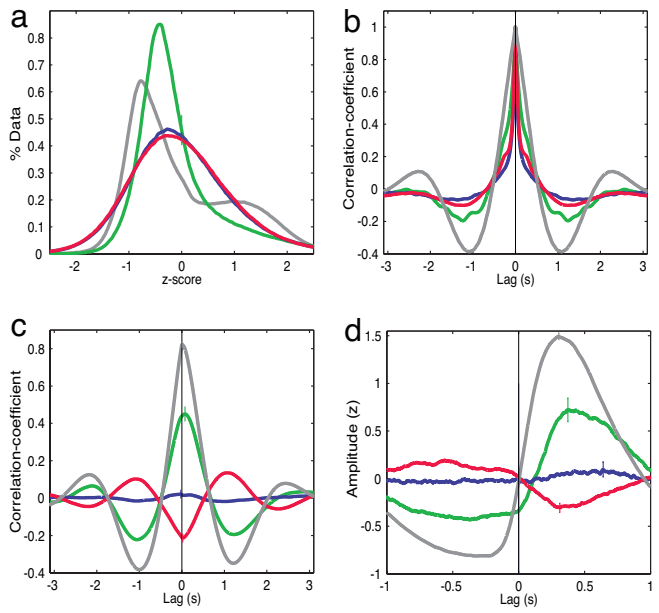

Fig. 4. Comparisons of the UDS responses of the three hippocampal subfields and cortical LFP. (*a*) MP histograms. Dentate gyrus granule cells show a weakly bimodal distribution (green), whereas CA1 (red) and CA3 (blue) pyramidal neurons show unimodal distributions. In comparison, the LFP histogram (gray) shows strongly bimodal distribution. The same color scheme is used in the subsequent histograms. (*b*) MP autocorrelations. Whereas cortical LFP and granule cells' MP show a prominent slow oscillation of ≈0.5 Hz, CA1 neurons show a weaker modulation of that frequency range, and CA3 pyramidal neurons show the weakest modulation. (*c*) MP–LFP cross-correlations. The granule cells' MP is positively correlated with cortical LFP. CA3 pyramidal cells' MP is, on average, uncorrelated with cortical LFP. CA1 pyramidal cells' MP is anticorrelated with cortical LFP. For comparison, the cross-correlation between the LFPs recorded from dorsal CA1 and layer two/three parietal cortex is also shown (gray). The LFP–LFP correlation reached a maximum of 0.72 ± 0.02 at a latency of 26 ± 8 ms ($P = 1e^{-3}$), indicating that the UDS in CA1 LFP occurred after parietal LFP. (*d*) LFP-triggered MP. Granule cells get rapidly depolarized shortly after the cortical LFP makes a transition to the up state (gray). The population of CA3 pyramidal cells does not show a transition, whereas CA1 pyramidal cells get less depolarized following a cortical transition to the up state. Small, colored vertical lines in *a*, *c*, and *d* indicate standard errors of the mean.

more, the responses of dentate gyrus, CA3, and CA1 are probably dependent on several other parameters such as the depth of SWS, the anesthetic, and the behavioral state (28). Finally, the precise timing of CA3 spikes could profoundly alter the CA1 response to entorhinal activity (34, 36).

These mechanisms could potentially explain some of the differences between the findings presented here and two related studies that have been published since the submission of this work. One study simultaneously measured the LFP in CA1 and the MP in various parts of the cortico-hippocampal circuit by using sharp electrodes (37). They found that CA3 pyramidal neurons were consistently less depolarized during the up state and that CA1 pyramidal neurons showed both an increase and a decrease in their depolarization during the down state. We find a mixed increase and decrease in CA3 depolarization and a consistent reduction in CA1 depolarization during the up state. In addition to the factors listed above, other factors could contribute to these differences, such as the site of the LFP electrode (CA1 versus parietal cortex) or the reference electrode (11), the technique of intracellular measurements (sharp electrodes versus whole-cell), and species-specific differences in the reaction to the anesthetic (rat versus mouse). Furthermore, the nature of UDS and analysis methods differ across studies. In our experiments, the UDS frequency is ≈0.4 Hz whereas in ref. 37 it is ≈0.8 Hz, perhaps reflecting differences in the levels of anesthesia. Furthermore, the LFP in our studies shows a bimodal distribution (Fig. 4*a* and SI Fig. 5) (35) with a sharp transition to the up state, whereas the LFP is unimodal in (37). Additionally, we computed the cross-correlation between the parietal cortical LFP and MP and the LFP-triggered average of MP, whereas several other measures, such as the joint probability distribution of the MP and the second principal component of the CA1 LFP, are used in ref. 37. Finally, all of our MP recordings were synchronized with respect to the same reference LFP in layer two/three of parietal cortex that sends input to the hippocampus, whereas some of the MP measurements in ref. 37, such as the granule cells' MP, were not carried out with respect to the same LFP reference.

Another study reported increased multiunit activity in layer five of the visual cortex, 50 ms before increased multiunit activity in CA1 in rats during SWS (38). This finding is consistent with our observation of a 72 ms phase lag of hippocampal LFP compared with the parietal LFP (Fig. 4*c*). However, we find a decrease in CA1 pyramidal neurons' activity when the parietal cortical neurons are more active in the up state. Furthermore, hippocampal neurons fire at an elevated rate during the ripples. Consistent with our findings, a recent study found that CA1 ripple occurrence was increased during cortical down state just before the neocortical multiunit activity made a transition to the up state (25). However, another study reported reduced occurrence hippocampal ripples during and just before the prefrontal LFP made a transition to the down state (11). Furthermore, ref. 24 found that ripple probability and hippocampal multiunit activity increased after the onset of up state in the cortex, and ref. 37 reported a mixed response of CA1 pyramidal neurons during cortical up state.

All of the factors listed in the previous paragraphs could contribute to the differences between these studies. In addition, the nature of UDS and the composition of multiunit activity could contribute. The quiet periods in refs. 11 and 38, reminiscent of the down state, were short (≈0.2 s), and the active periods, reminiscent of the up state, were longer (≈1 s). In contrast, in our studies, the down states were long (≈1.5 s), and the up states were shorter (≈0.5 s). It is conceivable that with longer up states, indicative of larger levels of depolarization, the CA1 pyramidal neurons increase firing rate during the up state. Furthermore, both pyramidal neurons and inhibitory interneurons could contribute to the hippocampal multiunit activity. CA1 interneurons show UDS that are phase locked to cortical UDS with a short delay (35). These interneurons spike at much higher rates (0.41 Hz) than the CA1 pyramidal neurons (0.14 Hz), and they increase their firing rates during the up state. Depending on the relative contributions of interneuronal and pyramidal neuronal spikes to the multiunit activity, the CA1 multiunit activity can have a different relationship with cortical UDS.

Our results are unexpected for two reasons. First, previous reports indicate that when the neocortex shows UDS, the hippocampus shows uncorrelated activity called large irregular activity (19, 20), whereas we find that the principal neurons in dentate gyrus, the hippocampal input region, as well as neurons in the hippocampal output region CA1, are phase locked to neocortical UDS. Second, it has been hypothesized that the hippocampus drives the neocortex during SWS (25). In contrast, our results suggest that neocortical activity propagates through the hippocampus in a dissipating and partly inhibitory fashion (35). The differential response of principal neurons in the hippocampal subfields could contribute to the hypothesized consolidation (1–11) or transformation (12) of recently learned information (39, 40) during sleep.

Materials and Methods

Animals, Surgery, and Histology. All methods were similar to those described in Hahn *et al.* (35). Briefly, data were obtained from 33 C57BL6 mice aged postnatal day (p)26 to p41 (p35 ± 0.6) weighing 12–21 g (17.5 ± 0.4 g). Mice were anesthetized with urethane (1.6–2.2 g/kg i.p.). After electrophysiological recordings, mice were transcardially perfused with 0.1 M PBS followed by 4% paraformaldehyde and 150- to 200-μm thick coronal brain sections were processed with the avidin–biotin–peroxidase method. Unidentified neurons were excluded from analysis. Figs. 1*b*, 2*b*, and 3*b* were generated by taking an image stack of the slice containing the cell soma and applying a minimum intensity projection on that stack. All experimental procedures were carried out according to the animal welfare guidelines of the Max Planck Society.

Electrophysiology and Data Acquisition. LFPs were recorded with a 16-site single-shank probe (NeuroNexus Technologies, Ann Arbor, MI). LFP from layer two/three of parietal cortex (2.0 mm, posterior to bregma; 1.5 mm, lateral) was used for all of the analyses in this study. *In vivo* intracellular MP was recorded in whole-cell configuration by using borosilicate glass patch pipettes with dc resistances of 4–8 MΩ and filled with a solution containing 135 mM potassium gluconate, 4 mM KCl, 10 mM Hepes, 10 mM phosphocreatinine, 4 mM MgATP, 0.3 mM Na3GTP (adjusted to pH 7.2 with KOH), and 0.2% biocytin for histological identification. Whole-cell recording configuration was achieved as described in ref. 41. Relative to bregma, the craniotomy for the MP recordings was made at 1–2.5 mm posterior and at 1–3 mm lateral. Average series resistance during the whole-cell recordings was 72 ± 4.4 MΩ. No current injections were made. MP was not corrected for the junction potential of approximately +7 mV. Both LFP and MP were recorded continuously on an eight-channel Cheetah acquisition system (Neuralynx, Tucson, AZ) for at least 900 s per experiment. The complete recording was used for subsequent analysis. MP was acquired by Axoclamp-2B (Axon Instruments, Union City, CA) and fed into a Lynx-8 amplifier (Neuralynx). LFP was recorded by an HS16 preamplifier (Neuralynx). LFP was sampled at 2 kHz, low-pass filtered at 250 Hz, and amplified 1,000–4,000 times. MP was low-pass filtered at 9 kHz, sampled at 32 kHz, and amplified 50–150 times. Simultaneously, MP was recorded by an ITC18 interface (Instrutech, Mineola, NY) under the control of Pulse software (Heka, Lambrecht, Germany).

Data Analysis. Data were detrended, converted to dimensionless units of *z* score, and used to compute MP histograms, auto- and cross-correlations, and MP–LFP correlation as described in Hahn *et al.* (35). When not specified, tests of significance are done with the Student's *t* test. Otherwise, significance was tested with nonparametric binomial tests (42).

We thank O. Ahmed, R. Burwell, D. Haydon-Wallace, J. Kauer, and S. Schnall for a careful reading of the manuscript; M. Kaiser for expert technical assistance; M. Oberlaender and P. Broser for assistance with histology panels; and J. Kauer and M. Blatow for advice on identification of histological reconstructions. M.R.M. was supported by the Rhode Island Foundation, the Salomon Foundation, a National Institutes of Health/Collaborative Research in Computational Neuroscience grant, a Young Investigator Award from the National Alliance for Research on Schizophrenia and Depression Foundation, and a Faculty Early Career Award from the National Science Foundation.

1. Marr D (1971) *Philos Trans R Soc London B* 262:23–81.
2. Milner B (1972) *Clin Neurosurg* 19:421–446.
3. Scoville WB, Milner B (2000) *J Neuropsychiatry Clin Neurosci* 12:103–113.
4. Wilson MA, McNaughton BL (1994) *Science* 265:676–679.
5. Skaggs WE, McNaughton BL (1996) *Science* 271:1870–1873.
6. Qin YL, McNaughton BL, Skaggs WE, Barnes CA (1997) *Philos Trans R Soc Lond B* 352:1525–1533.
7. Nadasdy Z, Hirase H, Czurko A, Csicsvari J, Buzsaki G (1999) *J Neurosci* 19:9497–9507.
8. Louie K, Wilson MA (2001) *Neuron* 29:145–156.
9. Lee AK, Wilson MA (2002) *Neuron* 36:1183–1194.
10. Alvarez P, Squire LR (1994) *Proc Natl Acad Sci USA* 91:7041–7045.
11. Molle M, Yeshenko O, Marshall L, Sara SJ, Born J (2006) *J Neurophysiol* 96:62–70.
12. Mehta MR (2007) *Nat Neurosci* 10:13–15.
13. Steriade M, Contreras D, Curro Dossi R, Nunez A (1993) *J Neurosci* 13:3284–3299.
14. Cowan RL, Wilson CJ (1994) *J Neurophysiol* 71:17–32.
15. Steriade M, Timofeev I, Grenier F (2001) *J Neurophysiol* 85:1969–1985.
16. Petersen CC, Hahn TT, Mehta M, Grinvald A, Sakmann B (2003) *Proc Natl Acad Sci USA* 100:13638–13643.
17. Leger JF, Stern EA, Aertsen A, Heck D (2005) *J Neurophysiol* 93:281–293.
18. Burwell RD, Amaral DG (1998) *J Comp Neurol* 398:179–205.
19. Vanderwolf CH (1969) *Electroencephalogr Clin Neurophysiol* 26:407–418.
20. O'Keefe J, Nadel L (1978) *The Hippocampus as a Cognitive Map* (Clarendon, Oxford).
21. Jones MW, Wilson MA (2005) *PLoS Biol* 3:e402.
22. Siapas AG, Lubenov EV, Wilson MA (2005) *Neuron* 46:141–151.
23. Siapas AG, Wilson MA (1998) *Neuron* 21:1123–1128.
24. Sirota A, Csicsvari J, Buhl D, Buzsaki G (2003) *Proc Natl Acad Sci USA* 100:2065–2069.
25. Battaglia FP, Sutherland GR, McNaughton BL (2004) *Learn Mem* 11:697–704.
26. Wolansky T, Clement EA, Peters SR, Palczak MA, Dickson CT (2006) *J Neurosci* 26:6213–6229.
27. Amaral DG, Witter MP (1995) *The Rat Nervous System* (Academic, San Diego).
28. Winson J, Abzug C (1977) *Science* 196:1223–1225.
29. Mizumori SJ, McNaughton BL, Barnes CA (1989) *J Neurophysiol* 61:15–31.
30. Jung MW, McNaughton BL (1993) *Hippocampus* 3:165–182.
31. Csicsvari J, Hirase H, Mamiya A, Buzsaki G (2000) *Neuron* 28:585–594.
32. Destexhe A, Contreras D, Steriade M (1999) *J Neurosci* 19:4595–4608.
33. Kehl SJ, McLennan H (1985) *Exp Brain Res* 60:309–317.
34. Dvorak-Carbone H, Schuman EM (1999) *J Neurophysiol* 82:3213–3222.
35. Hahn TT, Sakmann B, Mehta MR (2006) *Nat Neurosci* 9:1359–1361.
36. Ang CW, Carlson GC, Coulter DA (2005) *J Neurosci* 25:9567–9580.
37. Isomura Y, Sirota A, Ozen S, Montgomery S, Mizuseki K, Henze DA, Buzsaki G (2006) *Neuron* 52:871–882.
38. Ji D, Wilson M (2007) *Nat Neurosci* 10:100–107.
39. Mehta MR, Quirk MC, Wilson MA (2000) *Neuron* 25:707–715.
40. Mehta MR, Barnes CA, McNaughton BL (1997) *Proc Natl Acad Sci USA* 94:8918–8921.
41. Margrie TW, Brecht M, Sakmann B (2002) *Pflugers Arch* 444:491–498.
42. Zar JH (1999) *Biostatistical Analysis* (Prentice–Hall, Englewood Cliffs, NJ).